Monthly Notices of the ROYAL ASTRONOMICAL SOCIETY

Mon. Not. R. Astron. Soc. **412,** 2277–2285 (2011) doi:10.1111/j.1365-2966.2010.18051.x

Which haloes host *Herschel*-ATLAS galaxies in the local Universe?

Qi Guo,[1★] Shaun Cole,[1] Cedric G. Lacey,[1] Carlton M. Baugh,[1] Carlos S. Frenk,[1] Peder Norberg,[2] R. Auld,[3] I. K. Baldry,[4] S. P. Bamford,[5] N. Bourne,[5] E. S. Buttiglione,[6] A. Cava,[7] A. Cooray,[8] S. Croom,[9] A. Dariush,[3] G. De Zotti,[6,10] S. Driver,[11] L. Dunne,[5] S. Dye,[3] S. Eales,[3] J. Fritz,[12] A. Hopkins,[13] R. Hopwood,[14] E. Ibar,[15] R. J. Ivison,[15] M. Jarvis,[16] D. H. Jones,[13] L. Kelvin,[11] J. Liske,[17] J. Loveday,[18] S. J. Maddox,[5] H. Parkinson,[2] E. Pascale,[3] J. A. Peacock,[2] M. Pohlen,[3] M. Prescott,[4] E. E. Rigby,[5] A. Robotham,[11] G. Rodighiero,[6] R. Sharp,[13] D. J. B. Smith,[3] P. Temi[19] and E. van Kampen[17]

[1]*Department of Physics, Institute for Computational Cosmology, University of Durham, South Road, Durham DH1 3LE*
[2]*SUPA, Institute for Astronomy, University of Edinburgh, Royal Observatory, Blackford Hill, Edinburgh EH9 3HJ*
[3]*School of Physics & Astronomy, Cardiff University, Queens Buildings, The Parade, Cardiff CF24 3AA*
[4]*Astrophysics Research Institute, Liverpool John Moores University, Twelve Quays House, Egerton Wharf, Birkenhead CH41 1LD*
[5]*School of Physics and Astronomy, University of Nottingham, Nottingham NG7 2RD*
[6]*INAF - Osservertorio Astronomico di Padova, Vicolo Osservatorio 5, I-35122 Padova, Italy*
[7]*Instituto de Astrofsica de Canarias (IAC) and Departamento de Astrofisica de La Laguna (ULL), La Laguna, Tenerife, Spain*
[8]*Department of Physics and Astronomy, University of California, Irvine, CA 92697, USA*
[9]*Sydney Institute for Astronomy, School of Physics, University of Sydney, NSW 2006, Australia*
[10]*SISSA, Via Bonomea 265, I-34136 Trieste, Italy*
[11]*School of Physics and Astronomy, University of St Andrews, North Haugh, St Andrews, Fife KY16 9SS*
[12]*Sterrenkundig Observatorium, Universiteit Gent, Krijgslaan 281 S9, B-9000 Gent, Belgium*
[13]*Australian Astronomical Observatory, PO Box 296, Epping, NSW 1710, Australia*
[14]*Department of Physics and Astronomy, The Open University, Walton Hall, Milton Keynes MK7 6AA*
[15]*UK Astronomy Technology Centre, Royal Observatory, Edinburgh EH9 3HJ*
[16]*Centre for Astrophysics, Science & Technology Research Institute, University of Hertfordshire, Hatfield, Herts AL10 9AB*
[17]*European Southern Observatory, Karl-Schwarzschild-Strasse 2, D-85748 Garching bei Munchen, Germany*
[18]*Astronomy Centre, University of Sussex, Falmer, Brighton BN1 9QH*
[19]*Astrophysics Branch, NASA Ames Research Center, Mail Stop 2456, Moffett Field, CA 94035, USA*

Accepted 2010 November 19. Received 2010 November 19; in original form 2010 September 3

ABSTRACT

We measure the projected cross-correlation between low-redshift ($z < 0.5$) far-infrared selected galaxies in the science demonstration phase (SDP) field of the *Herschel*-ATLAS (H-ATLAS) survey and optically selected galaxies from the Galaxy and Mass Assembly (GAMA) redshift survey. In order to obtain robust correlation functions, we restrict the analysis to a subset of 969 out of 6900 H-ATLAS galaxies, which have reliable optical counterparts with $r < 19.4$ mag and well-determined spectroscopic redshifts. The overlap region between the two surveys is 12.6 deg^2; the matched sample has a median redshift of $z \approx 0.2$. The cross-correlation of GAMA and H-ATLAS galaxies within this region can be fitted by a power law, with correlation length $r_0 \approx 4.63 \pm 0.51$ Mpc. Comparing with the corresponding autocorrelation function of GAMA galaxies within the SDP field yields a relative bias (averaged over 2–8 Mpc) of H-ATLAS and GAMA galaxies of $b_{\rm H}/b_{\rm G} \approx 0.6$. Combined with clustering measurements from previous optical studies, this indicates that most of the low-redshift H-ATLAS sources are hosted by haloes with masses comparable to that of the Milky Way. The correlation function appears

★E-mail: qi.guo@durham.ac.uk

to depend on the 250-μm luminosity, L_{250}, with bright (median luminosity $\nu L_{250} \sim 1.6 \times 10^{10}\,\mathrm{L_{\odot}}$) objects being somewhat more strongly clustered than faint ($\nu L_{250} \sim 4.0 \times 10^{9}\,\mathrm{L_{\odot}}$) objects. This implies that galaxies with higher dust-obscured star formation rates are hosted by more massive haloes.

Key words: galaxies: haloes – dark matter – infrared: galaxies.

1 INTRODUCTION

It is well known that L^* galaxies are the largest contributors to the present-day stellar mass density (e.g. Li & White 2009). It is, however, not clear how star formation is distributed across galaxies and haloes of different masses. Previous studies show that in the local Universe star formation takes place preferentially in low-density environments (e.g. Lewis et al. 2002; Heinis et al. 2009). The most commonly used estimators of the star formation rate (SFR) are based on the ultraviolet (UV) continuum, or Hα, Hβ or [O II] emission lines (e.g. Brinchmann et al. 2004; Salim et al. 2007). These are all subject to uncertain dust extinction corrections and so can greatly underestimate the SFRs in dust-obscured regions. Mid- and far-infrared (far-IR) observations, which are sensitive to the energy re-emitted by dust heated by young stars, are therefore an essential complement to UV and optical tracers of star formation. Such dust is heated to temperatures of around 20–40 K, emitting thermal radiation, which peaks at wavelengths around 100 μm. The *IRAS* measured the far-IR emission from bright galaxies, but more recent surveys of dust emission have focused on either mid-IR (*ISO*, *Spitzer)* or submillimetre (e.g. SCUBA) wavelengths, missing the peak in the dust emission, and therefore requiring uncertain extrapolations to infer total IR luminosities and hence dust-obscured SFRs. The launch of *Herschel* (Pilbratt et al. 2010) has now opened up the study of the Universe at far-IR wavelengths (60–700 μm), spanning the peak of the dust emission from star-forming galaxies and allowing robust measurements of the dust-obscured SFR. The *Herschel*-ATLAS (H-ATLAS) survey (Eales et al. 2010) will provide far-IR imaging and photometry covering the wavelength range from 110 to 500 μm, over an area of 550 deg^2, much larger than previous surveys at these wavelengths, such as the *BLAST* (Devlin et al. 2009).

Analysis of clustering statistics provides a simple but powerful way to investigate environmental effects, in this case the SFR of galaxies. In this paper, we perform a preliminary clustering analysis of a 4×4 deg^2 field observed during the H-ATLAS science demonstration phase (SDP). Previous analyses of the H-ATLAS (Maddox et al. 2010) and HerMES (Cooray et al. 2010) surveys have focused on angular autocorrelations, with no significant signal in the former case and a significant detection in the latter. The clustering of galaxies at wavelengths of 250–500 μm was previously studied by Viero et al. (2009) using the angular power spectrum of data from the *BLAST* survey. Here, we consider spatial cross-correlations of far-IR and optical galaxies, which can be used to derive the clustering bias and hence the characteristic mass of the host haloes. We analyse a sample of ∼1000 H-ATLAS galaxies, which have reliable counterparts brighter than $r < 19.4$ mag in the Sloan Digital Sky Survey (SDSS) and spectroscopic redshifts measured by the Galaxy and Mass Assembly (GAMA) survey.[1] Presently, the overlap region between the H-ATLAS and GAMA surveys is 12.6 deg^2 and the spectroscopic redshift completeness is 99.7 per cent for galaxies with $r < 19.4$ mag.

A full analysis of the spatial autocorrelation function of H-ATLAS galaxies is given in van Kampen et al. (in preparation). Here we instead measure the cross-correlation function of H-ATLAS and GAMA galaxies, a statistic that provides a more robust and accurate estimate of the clustering bias of the H-ATLAS galaxies. There are at least two reasons why this is so. First, the sample of the H-ATLAS in the relatively small SDP survey area is small. In contrast, the number of GAMA galaxies in this area exceeds that of H-ATLAS galaxies by a factor of ∼10. Secondly, the redshift distribution of the GAMA galaxies can be robustly measured from the full GAMA survey (rather than from just the restricted SDP area) and for the estimator we employ, knowledge of the H-ATLAS redshift distribution is not required. Thus, the systematic uncertainties due to cosmic variance are reduced. As a result, the estimate of the cross-correlation function of the relatively sparse H-ATLAS sample with the more populous GAMA sample has much better statistics than the estimate of the H-ATLAS autocorrelation function alone. Finally, even though our sample is relatively small, using the cross-correlation technique allows us to investigate the dependence of clustering on far-IR luminosity by dividing the H-ATLAS sample into two subsets according to 250 μm luminosity. In this manner, we determine the clustering bias and infer the typical halo mass for each subset.

Throughout this paper, we assume a flat Λ cold dark matter (ΛCDM) cosmology with $\Omega_{\mathrm{m}} = 0.25, \Omega_{\Lambda} = 0.75$ and $H_0 = 73\,\mathrm{km\,s^{-1}\,Mpc^{-1}}$.

2 SAMPLE SELECTION

We use data obtained by the Spectral and Photometric Imaging Receiver (SPIRE, Griffin et al. 2010; Pascale et al. 2010) in the 16-deg^2 H-ATLAS science demonstration field.[2] In total there are 6878 sources over an area of 14.4 deg^2 that are brighter than the 5σ detection limit in one or more of the three SPIRE bands: 250, 350 and 500 μm (Rigby et al. 2010). The corresponding flux limits are 33, 36 and 45 mJy beam^{-1}. Below we work with the 250-μm flux-limited sample as this is the most-sensitive band, has the best positional accuracy and was used for source detection in the catalogue that was matched to the GAMA (Smith et al. 2010).

A significant fraction of these 6878 *Herschel* galaxies lie at low redshifts and have optical counterparts in the SDSS imaging

[1] The GAMA will eventually provide a highly complete, wide-area spectroscopic survey of over 400 000 galaxies with subarcsecond optical/near-IR imaging (from the SDSS, UKIDSS, VST and VISTA) and complementary observations from the UV (*GALEX*) to the mid- and far-IR (*WISE*, *Herschel*) and the radio (ASKAP, GMRT). The GAMA has so far surveyed 144 deg^2 and the catalogue contains 95 000 galaxy redshifts to r-band magnitude 19.4 with a redshift completeness of 98.7 per cent (Driver et al. 2009; Driver et al. 2010; Baldry et al. 2010; Hill et al. 2010; Robotham et al. 2010).

[2] PACS data (Ibar et al. 2010) are also available but are not used here.

catalogue. Sources with signal-to-noise ratio ≥5 at 250 μm (6621) were matched to the r-band-selected ($r < 22.4$) SDSS catalogue by Smith et al. (2010) using a likelihood ratio analysis (Sutherland & Saunders 1992; Ciliegi et al. 2003) with a maximum 10 arcsec search radius. This leads to 4756 sources, which have at least one candidate optical counterpart in the SDSS. A reliability value ($R_{\rm LR}$) is then assigned to each of the optical candidates, which quantifies the probability that the counterpart is a genuine match. We discard candidates with $R_{\rm LR} < 0.8$ to remove unreliable matches, leaving 2424 reliably matched sources. The angular overlap of the GAMA 9-h field with the H-ATLAS is not perfect and this reduces the survey region (hereinafter GAMA-SDP) from 14.4 to 12.6 deg^2. Within this region there are 2143 reliably matched sources. The spectroscopic redshift coverage of the GAMA in this region is complete at 99.7 per cent for an r-band Petrosian magnitude (corrected for Galactic extinction) brighter than 19.4 mag. Imposing this cut leaves 969 galaxies, which have measured spectroscopic redshifts and form the sample we analyse below (the H-ATLAS sample). A statistical analysis of the excess number of close pairs shows that 16 per cent of GAMA sources brighter than 19.4 mag have a H-ATLAS counterpart; of these, ∼80 per cent have directly identified reliable matches (Smith et al. 2010). We only have spectroscopic redshifts for H-ATLAS galaxies that have reliable matches in the r-band-limited GAMA survey. Hence, while we believe we have a complete representative sample of the local H-ATLAS galaxies, we could, in principle, be missing galaxies which are bright at 250 μm but too faint for detection in the r band. This possibility cannot be ruled out until we have spectroscopic redshifts selected in the submillimetre.

To k-correct the observed *Herschel* fluxes to the rest-frame 250 μm, we assume that the dust emission has a spectral energy distribution of the form

$$L_\nu \propto B_\nu(T)\,\nu^\beta, \tag{1}$$

where $B_\nu(T)$ is the Planck function. There are two parameters in this formula: the dust temperature, T, and the emissivity index, β. We adopt the values, $T = 28$ K and $\beta = 1.5$, derived by Amblard et al. (2010) by fitting to nearby H-ATLAS galaxies detected in at least three far-IR bands with a significance greater than 3σ.

The luminosity distribution at 250 μm (L_{250}) is shown in Fig. 1. It peaks at around $L_{250} = 3.2 \times 10^{24}$ W Hz^{-1}, corresponding to the local L^* galaxies found by Dye et al. (2010). We further split the H-ATLAS sample into two subsets (indicated by the vertical dotted line in Fig. 1): bright sources with $L_{250} > 2.5 \times 10^{24}$ W Hz^{-1} [corresponding to total IR luminosity, $L_{\rm IR} = 5.0 \times 10^{10}\,{\rm L}_\odot$, based on equation (1), integrating from 8 to 1000 μm] and faint sources with $L_{250} < 2.5 \times 10^{24}$ W Hz^{-1}. The faint subset consists of 484 galaxies and the bright one consists of 485 galaxies. The median values of L_{250} for the faint and bright H-ATLAS subsamples are 1.3×10^{24} and 5.0×10^{24} W Hz^{-1}, respectively (corresponding to total IR luminosities of 2.5×10^{10} and $7.9 \times 10^{10}\,{\rm L}_\odot$), so that they differ by a factor of 3 in typical luminosity. Fig. 2 shows the number counts as a function of the 250-μm flux. Although these two subsets are well distinguished in luminosity, they have similar distributions of observed 250-μm flux.

The separation of the two samples by L_{250} is somewhat blurred by the uncertainties in the flux measurements and assumed k-corrections. Perturbing the luminosities according to the flux measurement errors in the H-ATLAS catalogue (Rigby et al. 2010) makes little difference with just 5 per cent of the sample switching from the bright to the faint subsets. The k-correction depends on the values of T and β assumed in equation (1). The sample of Amblard et al. (2010) spans the ranges $T = 28 \pm 8$ K and $\beta = 1.4 \pm 0.1$. This uncertainty can also scramble the luminosity subsets somewhat, but even the most extreme choice of $T = 36$ K and $\beta = 1.5$ only switches 8 per cent of the sample from the bright to the faint subsets. We return to the effect this might have on our clustering results in Section 3.

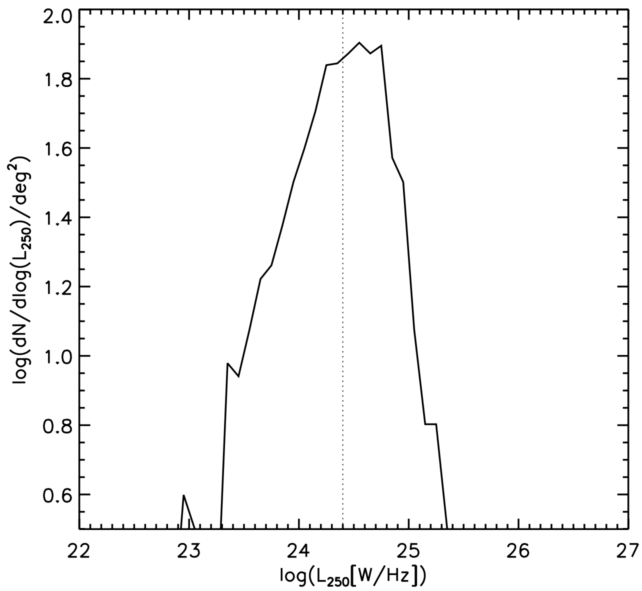

Figure 1. Observed distribution of *Herschel* 250-μm rest-frame luminosities for the 969 galaxies well matched to SDSS galaxies with $r < 19.4$ mag. The dotted line corresponds to the threshold (2.5×10^{24} W Hz^{-1}) used to split the sample into bright and faint subsets (see Section 2).

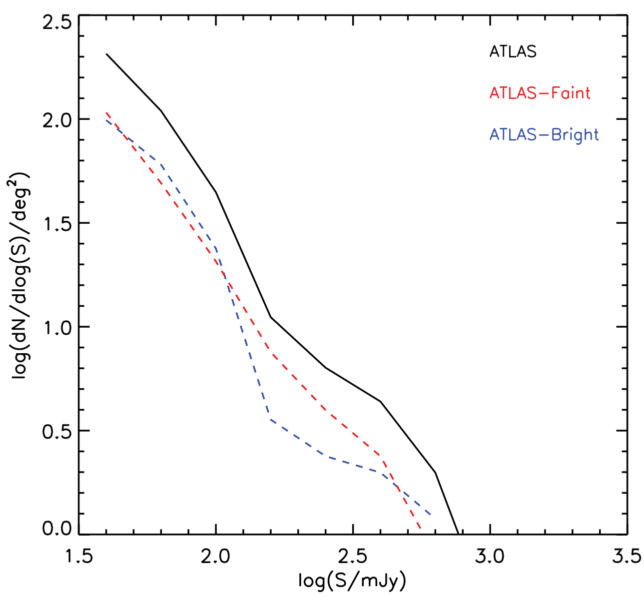

Figure 2. Flux distribution of *Herschel* sources at 250 μm. The blue and red-dashed curves are for the bright and faint *Herschel* sources, respectively, with the black line showing the combination of the two.

The distributions of apparent and absolute r-band magnitudes (corrected for Galactic dust extinction) are shown in Figs 3 and 4, respectively. The r-band absolute magnitudes have been k-corrected to $z = 0$ (Blanton et al. 2003). The r-band absolute magnitude for the full H-ATLAS sample peaks around −21.7, somewhat brighter than the Milky Way. For comparison, we also include the corresponding

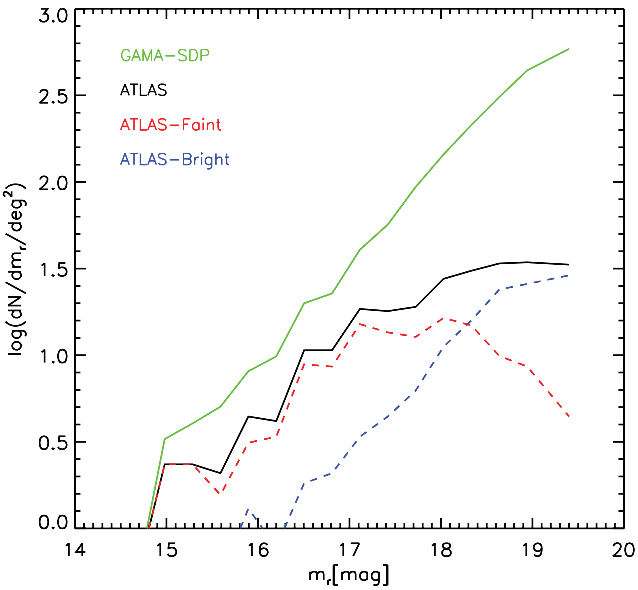

Figure 3. The r-band number counts per magnitude per square degree versus apparent magnitude. As in Fig. 2, the blue- and red-dashed curves are for the bright and faint H-ATLAS sources, and the black curve is the combination of the two. To compare, the green curve gives the number counts of all GAMA galaxies in the same region.

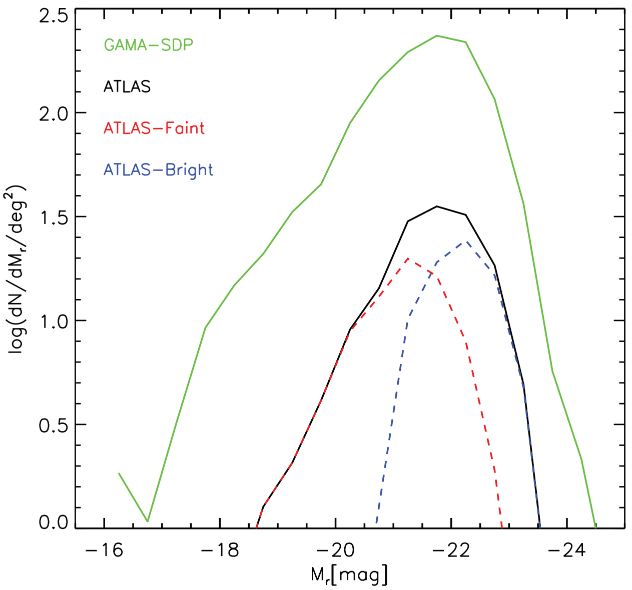

Figure 4. Similar to Fig. 3, but as a function of r-band absolute magnitude. The curves are colour-coded in the same way as in Fig. 3.

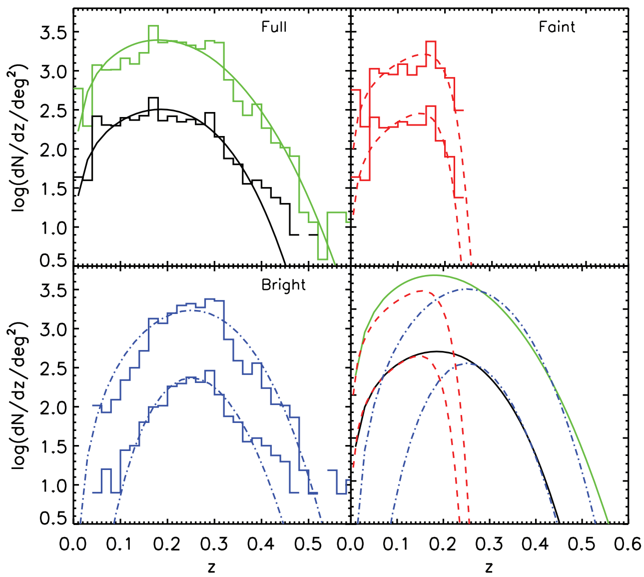

Figure 5. Redshift distributions of each of our samples, plotted as the number of galaxies per unit redshift per square degree. The colour-coding is as in Fig. 3: the red curves are for the H-ATLAS-faint and GAMA-faint samples, the blue curves are for the H-ATLAS-bright and GAMA-bright samples, the black curves are for the full H-ATLAS sample and the green curves are for the full GAMA sample. For the H-ATLAS, the histograms are the observed distributions and smooth curves are fits to these distributions. For the GAMA, the histograms show the redshift distribution of galaxies in the GAMA-SDP field, while smoothed curves are the fits to the full GAMA area. The fitted curves are collected in the bottom right-hand panel.

properties of the full GAMA sample in the same sky area in Figs 3 and 4. It can be seen that while there are more GAMA than H-ATLAS galaxies, their distributions of apparent and absolute r-band magnitude are similar. The extra galaxies in the GAMA catalogue may correspond to early-type and some late-type galaxies, for which the current SFRs are very low, leading to their absence from the far-IR survey. More detailed work on the properties of these galaxies is needed in the future.

The redshift distributions of our samples are shown in Fig. 5 as histograms. In each case, the upper histograms and curves correspond to the GAMA sample and the lower ones correspond to the H-ATLAS sample. As expected, the more luminous H-ATLAS galaxies tend to lie at higher redshifts. The redshift distributions of the luminous and faint galaxies cross at $z \sim 0.2$, which is roughly the median value for all the 969 H-ATLAS sources. To help interpret the cross-correlation of the faint and bright H-ATLAS sources with GAMA galaxies, we want subsets of the GAMA galaxies with similar redshift distributions to the corresponding H-ATLAS samples. To achieve this, we split the GAMA sample at $M_r = -21.2$ mag into faint and bright subsets. It can be seen in Fig. 5 that this choice of dividing magnitude results in the corresponding subsets of H-ATLAS and GAMA samples having very similar redshift distributions. The full, faint and bright GAMA samples have median absolute magnitudes M_r of -21.5, -20.5 and -22.0 mag, respectively.

3 CORRELATION FUNCTIONS

In this section, we first calculate the autocorrelation functions of the GAMA and H-ATLAS galaxies, then their cross-correlation, and finally the clustering bias of the H-ATLAS galaxies. The autocorrelation of the GAMA galaxies is needed for calculating the relative bias from the cross-correlation, while the H-ATLAS autocorrelation provides a consistency check on the results from the cross-correlation and also allows us to compare with the autocorrelation results of van Kampen et al. (in preparation).

3.1 Autocorrelation functions

In this section, we estimate the autocorrelation function of the GAMA and H-ATLAS SDP samples, and, for the H-ATLAS sample, the dependence of clustering strength on the *Herschel* 250-µm luminosity, L_{250}. We begin by considering the correlation function in redshift space, $\xi(r_\perp, r_\parallel)$, where $r_\perp$ and $r_\parallel$ are the comoving separations perpendicular and parallel to the line of sight, respectively, and integrate this over the line-of-sight separation, $r_\parallel$, to obtain the projected correlation function. This removes the effect of peculiar velocities on the estimate of the spatial correlation function.

There are several estimators for the autocorrelation function in the literature, all of which require the generation of a uniform random catalogue with the same mask as the galaxy catalogue itself. In this work, we adopt the estimator proposed by Hamilton (1993):

$$\xi(r_\perp, r_\parallel) = \frac{\mathrm{DD}(r_\perp, r_\parallel)\,\mathrm{RR}(r_\perp, r_\parallel)}{[\mathrm{DR}(r_\perp, r_\parallel)]^2} - 1, \tag{2}$$

where $\mathrm{DD}(r_\perp, r_\parallel)$, $\mathrm{DR}(r_\perp, r_\parallel)$ and $\mathrm{RR}(r_\perp, r_\parallel)$ are counts of data–data, data–random and random–random pairs, respectively. To generate smooth redshift distributions for the random samples, we fit their redshift distributions with the functional form

$$N(z) \propto z^\alpha \exp(-\beta z^\eta). \tag{3}$$

The fits to the redshift distributions of GAMA and H-ATLAS (sub)samples are shown as smooth curves in Fig. 5. To obtain a robust estimate of the mean redshift distribution of the GAMA galaxies, we made use of the full 144 deg^2 of the GAMA catalogue ($\sim 9 \times 10^4$ galaxies), rather than just the subset that overlaps with the H-ATLAS area ($\sim 7 \times 10^3$ galaxies). The completeness mask of Norberg et al. (2011) was used to generate the random catalogue corresponding to the GAMA sample.

Following standard practice, we estimate the projected correlation function, $w(r_\mathrm{p})$, by integrating equation (2) along the line-of-sight separation $r_\parallel$:

$$w(r_\mathrm{p}) = w(r_\perp) = \int_{-\infty}^{\infty} \xi(r_\perp, r_\parallel)\,\mathrm{d}r_\parallel. \tag{4}$$

In reality, we cannot integrate to infinity. Instead, we have chosen to integrate to ± 50 Mpc, but we test the impact of varying this limit. Errors are estimated using the Jackknife technique. We split each galaxy sample into 16 equal-area regions and then calculate the correlation functions for data taken from any 15 of these 16 regions. The scaled scatter of the Jackknife samples gives an estimate of the errors on the corresponding correlation functions (e.g. Norberg et al. 2009).

The projected correlation function is related to the real-space correlation function by a simple Abel transform (Davis & Peebles 1983). For a power law, $w(r_\mathrm{p}) = A r_\mathrm{p}^{1-\gamma}$, the 3D correlation function, $\xi(r)$, is also a power law, $\xi(r) = (r/r_0)^{-\gamma}$. The parameters are related by

$$r_0^\gamma = \frac{A\Gamma(\gamma/2)}{\Gamma(1/2)\Gamma[(\gamma-1)/2]}, \tag{5}$$

where $\Gamma(x)$ is the standard Gamma function.

The two-point projected autocorrelation functions are plotted in Fig. 6 as red curves. To test the convergence of the line-of-sight integral in equation (4), we show with green curves (here and later also in Fig. 7) the result of extending the integration out to 100 Mpc. The projected correlation function is seen to be insensitive to the precise choice of integration limit.

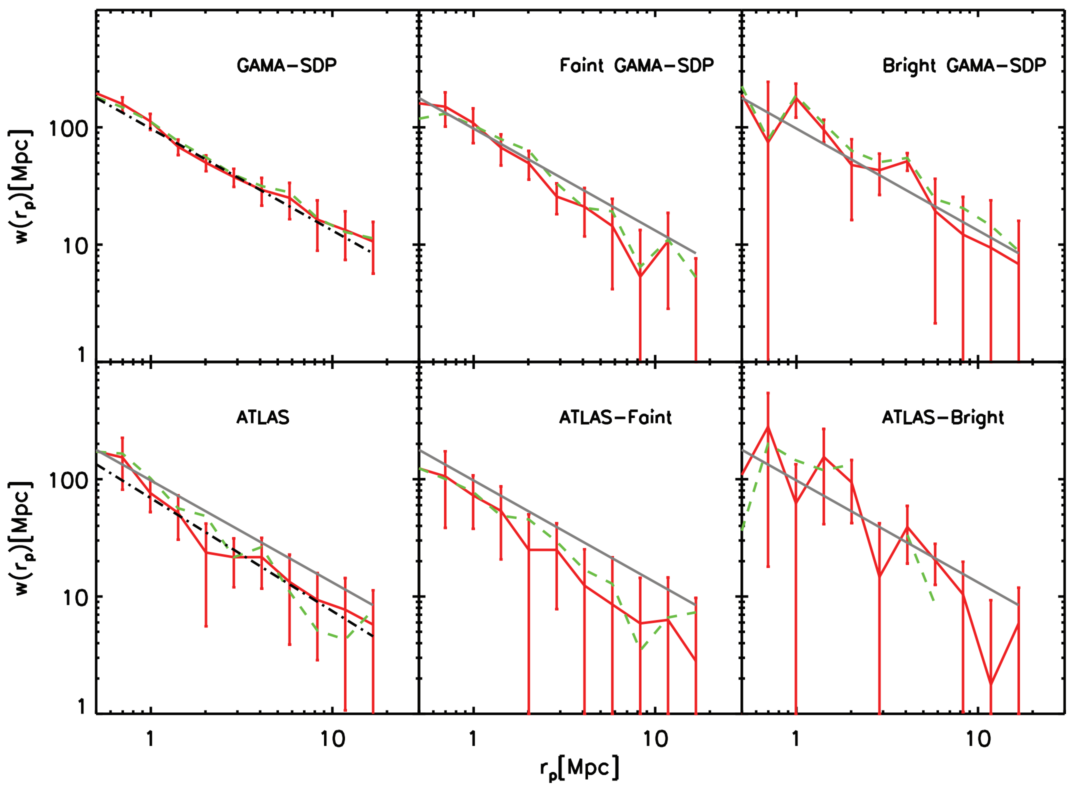

Figure 6. Two-point projected autocorrelation functions. From top to bottom, the panels correspond to GAMA, GAMA-faint and GAMA-bright samples (left-hand side), and to H-ATLAS, H-ATLAS-faint and H-ATLAS-bright samples (right-hand side). The red curves show the result of truncating the line-of-sight integration in equation (4) at 50 Mpc and the green dashed curves at 100 Mpc. The black dot–dashed lines are power-law fits to the data in red for full GAMA and H-ATLAS samples only. To aid comparison, the fit to the GAMA autocorrelation function for the full sample (top left-hand panel) is repeated as a grey curve in the other panels. Error bars are estimated using the Jackknife technique.

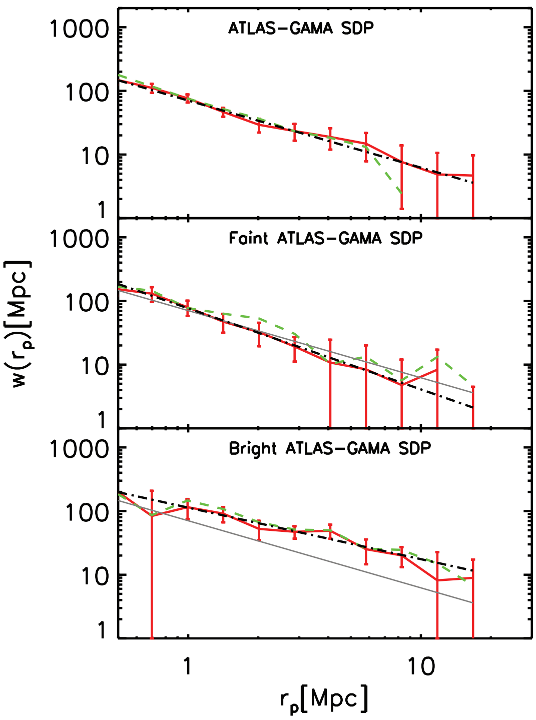

Figure 7. Two-point projected cross-correlation of all H-ATLAS with all GAMA galaxies (top panel), faint H-ATLAS with faint GAMA galaxies (middle panel) and bright H-ATLAS with bright GAMA galaxies (bottom panel). As in Fig. 6, the red curves show the result of integrating equation (4) to 50 Mpc and the green dashed curves show the result of integrating equation (4) to 100 Mpc. The black dot–dashed curves show the power-law fits to the red curves over the range 1–12 Mpc. For comparison, the fit to all the H-ATLAS–GAMA cross-correlation functions is replicated as grey lines in the lower two panels. Error bars are estimated using the Jackknife technique.

For the GAMA-SDP sample (top row), the projected correlation functions are measured in the region of overlap with the H-ATLAS. The reason for re-measuring the GAMA correlation functions in this restricted area rather than showing the less-noisy estimate from the full GAMA data set (Norberg et al., in preparation) is that we are interested in the relative clustering of H-ATLAS and GAMA galaxies and this choice will reduce the impact of sample variance on the comparison. The GAMA-SDP correlation function can be well fitted with a power law (black dot–dashed curve). Fitting equation (4) to the data in the range 1–12 Mpc and using equation (5), we find $r_0 = 5.96 \pm 0.62$ Mpc and $\gamma = 1.87 \pm 0.21$. This is consistent with the values for L^* optical galaxies (with $M_r^{0.1} \approx -21.1$) estimated in the SDSS: $r_0 = 6.6 \pm 0.3$ Mpc and $\gamma = 1.87 \pm 0.03$ (Zehavi et al. 2010).

The lower panels of Fig. 6 show the projected autocorrelation functions for our three H-ATLAS samples. The best-fitting values of r_0 and γ for these are summarized in Table 1. van Kampen et al. (in preparation) have carried out a more detailed analysis of the autocorrelation function of H-ATLAS galaxies using the angular correlations in redshift slices. They obtain a best estimate of the spatial clustering length, averaged over the redshift range $0.1 < z < 0.3$, of $r_0 = 5.5 \pm 0.9$ Mpc. Our estimate of r_0 given in Table 1 for the autocorrelation of our full H-ATLAS sample is consistent with this.

For comparison, the best-fitting power law for the GAMA-SDP autocorrelation function for the full GAMA sample is reproduced by a grey line in all of the other panels of Fig. 6. The full H-ATLAS sample is somewhat less clustered than the full GAMA-SDP sample. The faint H-ATLAS galaxies appear to have similar clustering to the full H-ATLAS sample, while the bright H-ATLAS galaxies appear to be more strongly clustered. However, the statistical uncertainties in the estimates for these small samples are clearly rather large and, moreover, systematic errors could be introduced by fitting smooth curves to their noisy redshift distributions. These limitations are largely overcome in the next section where we measure the clustering of the H-ATLAS galaxies by cross-correlating with the much larger GAMA-SDP sample. Furthermore, by estimating the GAMA-SDP radial selection function using the full GAMA survey covering an area about 10 times larger than the GAMA-SDP region, systematic uncertainties in the modelling of the radial selection function are significantly reduced.

In Fig. 6, it is apparent that our Jackknife error bars are sometimes noisy as witnessed, for example, by the large error bars at ∼0.7 Mpc or >6 Mpc for the GAMA bright sample or by the small error bars on the GAMA faint sample on scales below 2 Mpc. Further investigation has revealed that this is a result of our small sample and occurs because the clustering on particular scales can be dominated by one or two structures and so vary significantly in just one or two of our Jackknife samples. Such fluctuations are smaller for our cross-correlation samples, discussed below. Thus, the errors quoted for the correlation length, r_0, for the bright and faint GAMA autocorrelation samples have significant uncertainty, but the cross-correlation results and their error bars are more robust. The diagnostic tests used for the robustness of the clustering errors are similar to those presented in Norberg et al. (in preparation).

Table 1. The correlation length, r_0, and slope, γ, for the power-law fits to our auto- and cross-correlation functions and the mean redshift, z_{mean}, number of galaxies, N_{gal}, and relative bias of each sample.

Correlation function	r_0 (Mpc)	γ	z_{mean}	N_{gal}	Relative bias
GAMA-SDP auto	5.96 ± 0.62	1.87 ± 0.21	0.21	7761	
H-ATLAS auto	4.76 ± 0.63	1.96 ± 0.38	0.19	970	
Faint GAMA-SDP auto	5.19 ± 0.77	2.20 ± 0.43	0.13	1981	
Bright GAMA-SDP auto	7.06 ± 0.45	1.90 ± 0.27	0.26	4780	
Faint H-ATLAS auto	4.49 ± 1.05	2.15 ± 0.54	0.12	484	
Bright H-ATLAS auto	5.72 ± 0.53	2.06 ± 0.27	0.26	485	
H-ATLAS–GAMA cross	4.63 ± 0.51	2.05 ± 0.31			0.61 ± 0.08
Faint H-ATLAS–faint GAMA cross	4.38 ± 0.77	2.27 ± 0.47			0.67 ± 0.13
Bright H-ATLAS–bright GAMA cross	6.68 ± 0.44	1.81 ± 0.26			1.04 ± 0.22

3.2 Cross-correlation functions

The cross-correlation function in redshift space of H-ATLAS with GAMA galaxies is estimated using

$$\xi(r_\perp, r_\parallel) = \frac{\mathrm{HG}(r_\perp, r_\parallel)\,\mathrm{RR}(r_\perp, r_\parallel)}{\mathrm{HR}(r_\perp, r_\parallel)\,\mathrm{GR}(r_\perp, r_\parallel)} - 1, \tag{6}$$

where HG, HR, GR and RR are counts of H-ATLAS–GAMA, H-ATLAS–random, GAMA–random and random–random pairs, respectively. In each case, the random sample is generated so as to match the redshift distribution of the GAMA galaxies. Thus, for our estimates of the cross-correlation functions, at no point do we need to fit the noisy redshift distributions of the small samples of H-ATLAS galaxies. As for the autocorrelation functions, we calculate the projected two-point cross-correlation functions according to equation (4) and estimate the errors using the Jackknife technique.

The projected cross-correlation functions are shown in Fig. 7. The top panel shows the GAMA–H-ATLAS result when the limit of integration in equation (4) is taken to be 50 Mpc (red curves) and 100 Mpc (green curves). The dot–dashed line is the best-fitting power law to the 50-Mpc estimate. It shows that the H-ATLAS–GAMA cross-correlation function is well fitted by a power law, with $r_0 = 4.63 \pm 0.51$ Mpc and $\gamma = 2.05 \pm 0.31$, indicating that the clustering of the H-ATLAS galaxies is weaker than that of GAMA-SDP galaxies. This inferred difference between the strength of the H-ATLAS and GAMA-SDP clustering appears larger than suggested by comparing the upper and lower left-hand panels of Fig. 6 or the values of r_0 in Table 1. This might be the result of a bias in the redshift distribution of the random samples for the H-ATLAS galaxies, which is obtained by fitting a smooth function to noisy data (Section 3.1).

The lower panels in Fig. 7 show cross-correlation functions for subsets of luminous and faint H-ATLAS and GAMA galaxies. For comparison, this best-fitting line to the GAMA-H-ATLAS function is replicated in grey in these panels. Again, we find that the clustering of faint H-ATLAS galaxies is weaker than that of the bright galaxies. The estimates of r_0 and γ for these samples are summarized in Table 1.

As discussed in Section 2, there are uncertainties in the 250-μm k-correction and the flux measurements. Adopting the most-extreme perturbation to the k-corrections ($T = 36$ K and $\beta = 1.5$, see Section 2) and perturbing the fluxes according to the measurement errors quoted in Rigby et al. (2010) shifts the r_0 values of our estimated H-ATLAS autocorrelation functions by an amount comparable to the quoted 1σ statistical uncertainty. This variation is largely caused by the limited size of these samples and the resulting uncertainty in fitting their redshift distributions. The cross-correlations on which we focus and which do not depend on the redshift distributions of the H-ATLAS samples are much less affected by the uncertainties in the k-corrections and flux measurements. In this case, the same perturbations affect the r_0 values, by no more than 15 per cent of their quoted statistical error and so make a negligible contribution to the uncertainty in our results.

3.3 Bias of H-ATLAS galaxies

To interpret the meaning of the estimated large-scale cross-correlation functions, consider the simple linear bias model in which the auto- and cross-correlation functions of H-ATLAS and GAMA galaxies are related to the autocorrelation function, ξ_m, of the mass at redshift $z = 0$ by

$$\xi_\mathrm{H}(\boldsymbol{r}) = b_\mathrm{H}(z)^2\, D^2(z)\, \xi_\mathrm{m}(\boldsymbol{r}), \tag{7}$$

$$\xi_\mathrm{G}(\boldsymbol{r}) = b_\mathrm{G}(z)^2\, D^2(z)\, \xi_\mathrm{m}(\boldsymbol{r}), \tag{8}$$

$$\xi_\mathrm{HG}(\boldsymbol{r}) = b_\mathrm{H}(z) b_\mathrm{G}(z)\, D^2(z)\, \xi_\mathrm{m}(\boldsymbol{r}), \tag{9}$$

where the subscripts H and G denote H-ATLAS and GAMA, respectively, $D(z)$ is the linear growth factor of the perturbations in the mass and $\xi_\mathrm{m}(\boldsymbol{r})$ is the autocorrelation function of the dark matter. In this case, the projected cross-correlation function that we have estimated is related to that of the mass at $z = 0$ through

$$w_\mathrm{HG}(r_\mathrm{p}) = \langle b_\mathrm{H} b_\mathrm{G} D^2(z)\rangle\, w_\mathrm{m}(r_\mathrm{p}), \tag{10}$$

where the average product of the bias and growth factors is given by

$$\left\langle b_\mathrm{G} b_\mathrm{H} D^2(z)\right\rangle = \frac{\int \bar{n}_\mathrm{G}(z)\bar{n}_\mathrm{H}(z) b_\mathrm{G}(z) b_\mathrm{H}(z) D^2(z) \left(\frac{\mathrm{d}V}{\mathrm{d}z}\right) \mathrm{d}z}{\int \bar{n}_\mathrm{G}(z)\bar{n}_\mathrm{H}(z) \left(\frac{\mathrm{d}V}{\mathrm{d}z}\right) \mathrm{d}z}, \tag{11}$$

where $\bar{n}_\mathrm{H}(z)$ and $\bar{n}_\mathrm{G}(z)$ are the mean space densities of the H-ATLAS and GAMA samples, respectively, at redshift z. For the autocorrelation function of the GAMA galaxies, this reduces to

$$w_\mathrm{G}(r_\mathrm{p}) = \left\langle b_\mathrm{G}^2 D^2(z)\right\rangle w_\mathrm{m}(r_\mathrm{p}), \tag{12}$$

where

$$\left\langle b_\mathrm{G}^2 D^2(z)\right\rangle = \frac{\int \bar{n}_\mathrm{G}^2(z) b_\mathrm{G}^2(z) D^2(z) \left(\frac{\mathrm{d}V}{\mathrm{d}z}\right) \mathrm{d}z}{\int \bar{n}_\mathrm{G}^2(z) \left(\frac{\mathrm{d}V}{\mathrm{d}z}\right) \mathrm{d}z}. \tag{13}$$

The relative bias of the H-ATLAS and GAMA galaxies is then

$$b_\mathrm{HG}^\mathrm{rel} = w_\mathrm{GH}(r_\mathrm{p})/w_\mathrm{GG}(r_\mathrm{p}) = \left\langle b_\mathrm{H} b_\mathrm{G} D^2(z)\right\rangle / \left\langle b_\mathrm{G}^2 D^2(z)\right\rangle. \tag{14}$$

In principle, this depends on both the bias parameters b_H and b_G, and on $D(z)$. However, since by construction the redshift distributions of the full/faint/bright H-ATLAS samples match well with those of the corresponding (full/faint/bright) GAMA samples, the dependence on $D(z)$ will approximately cancel. If the bias parameters b_H and b_G evolve with redshift in the same way, then this evolution will also approximately cancel out in the relative bias. This is the reason why we cross-correlate H-ATLAS faint/bright with GAMA faint/bright instead of all GAMA galaxies.

We estimate the mean relative bias $\bar{b}_\mathrm{HG}^\mathrm{rel}$ of H-ATLAS and GAMA galaxies using

$$\bar{b}_\mathrm{HG}^\mathrm{rel} = \frac{\Sigma b_\mathrm{HG}^{\mathrm{rel},i}/\sigma_i^2}{\Sigma 1/\sigma_i^2}, \tag{15}$$

where $b_\mathrm{HG}^{\mathrm{rel},i}$ is obtained directly from the measured projected H-ATLAS–GAMA cross-correlation function and the GAMA autocorrelation function (rather than from the fits given in Table 1), and σ_i represents the Jackknife error on $b_\mathrm{HG}^{\mathrm{rel},i}$ estimated at each pair separation. This simple estimator ignores correlations between the measurements at different separations and so may not be optimal, but we do take account of such correlations in estimating the error on $\bar{b}_\mathrm{HG}^\mathrm{rel}$. Our error on $\bar{b}_\mathrm{HG}^\mathrm{rel}$ is estimated using the Jackknife technique by calculating the mean $b_{\mathrm{HG},j}^\mathrm{rel}$ for each Jackknife sample (assuming the same values of σ_i as used in equation 15) and then looking at the scatter in values between Jackknife samples.

Our estimates of $\bar{b}_\mathrm{HG}^\mathrm{rel}$ are shown in Fig. 8. For the full H-ATLAS and GAMA samples, the mean relative bias over the range of separations 2–8 Mpc, where the two-halo term dominates and where we have good statistics, is $b_\mathrm{HG}^\mathrm{rel}(\mathrm{all}) = 0.61 \pm 0.08$. Thus, we conclude that the clustering strength of H-ATLAS galaxies is significantly weaker than that of GAMA SDP galaxies. This important conclusion is revealed only by taking advantage of the cross-correlation function technique. As shown in Table 1, our estimates

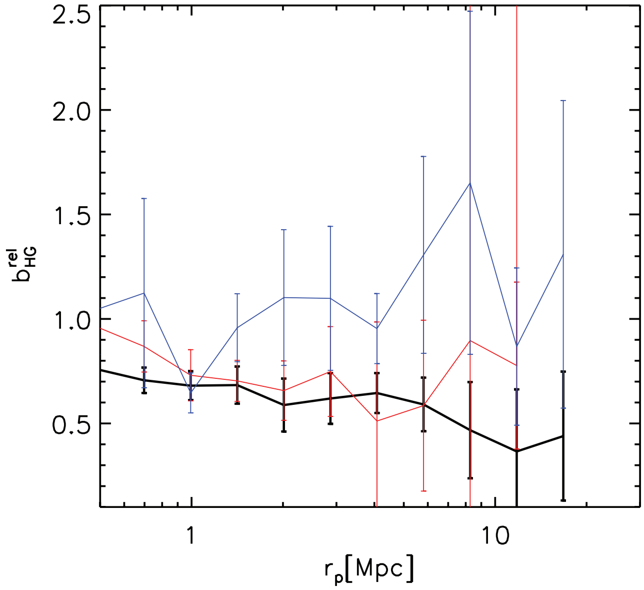

Figure 8. The relative bias $b^{\rm rel}_{\rm HG}$ estimated from the ratio of the projected H-ATLAS–GAMA cross-correlation function, $w_{\rm HG}(r_{\rm p})$, to the corresponding GAMA autocorrelation function $w_{\rm G}(r_{\rm p})$. The black curve is for the bias of the full H-ATLAS sample relative to the full GAMA sample, while the blue curve is for the bright H-ATLAS galaxies relative to bright GAMA galaxies, and the red curve is for faint H-ATLAS galaxies relative to faint GAMA galaxies. Errors are estimated using the Jackknife technique.

of the autocorrelation functions are much too noisy (and probably subject to systematic errors) to detect any difference between the two galaxy samples. From the cross-correlation of the faint H-ATLAS with the faint GAMA samples, we obtain a relative bias of $b^{\rm rel}_{\rm HG}({\rm faint}) = 0.67 \pm 0.13$, while from the cross-correlation of the bright H-ATLAS with the bright GAMA galaxies, we obtain $b^{\rm rel}_{\rm HG}({\rm bright}) = 1.04 \pm 0.22$.

To convert the estimates of relative bias into values of the absolute bias for the different H-ATLAS samples, we need to know the absolute bias of the different GAMA samples. For this we use the results of Zehavi et al. (2010) who measured the clustering as a function of r-band luminosity in the SDSS and combined that with a theoretical prediction for the clustering of the dark matter in the ΛCDM cosmology. An important qualification is that the values of bias measured by Zehavi et al. (2010) effectively apply at the average redshift of the SDSS, $z \sim 0.1$. The bias of r-band-selected galaxies is expected to evolve with redshift, but quantifying the size of this effect for the redshift range $z \lesssim 0.5$ probed in this paper must await a detailed clustering analysis of the full GAMA redshift survey. Here, we will simply assume that the bias factors for GAMA and H-ATLAS galaxies can be taken to be constant over the redshift range studied here. We therefore use equation (10) from Zehavi et al. (2010), scaled to $\sigma_8 = 0.8$, to calculate the value of the bias as a function of r-band absolute magnitude.

Our full, faint and bright GAMA samples have median absolute magnitudes $M_r^{0.1} = -21.3$, -20.3 and -21.8, respectively (k-corrected to $z = 0.1$ to be consistent with Zehavi et al. (2010)), implying average r-band bias factors of $b_{\rm G} = 1.17, 1.05$ and 1.29. This then leads to absolute bias values of $b_{\rm H} = 0.71 \pm 0.09$, 0.70 ± 0.14 and 1.34 ± 0.28, respectively, for the full, faint and bright H-ATLAS subsamples. We find that the bright H-ATLAS galaxies are more strongly clustered than the H-ATLAS population as a whole at the 2σ level, which confirms the trend seen from the H-ATLAS autocorrelation functions in Fig. 6. This result implies that the excess clustering of the bright H-ATLAS galaxies reflects a genuine and strong dependence of clustering on *far-IR luminosity* and thus on the SFR. We detect no significant difference between the bias of the faint H-ATLAS galaxies and that of the population as a whole. This result, however, could be affected by our assumption of a constant bias over the redshift of interest.

The final step is to use the estimated clustering bias of H-ATLAS galaxies to constrain the masses of the haloes hosting them. In the ΛCDM model at the present day, the halo bias is a very weak function of halo mass for haloes less massive than $10^{12}\,{\rm M}_\odot$ and increases rapidly with increasing halo mass at higher masses (Mo & White 2002). Using the fitting formula for bias as a function of halo mass at $z = 0$ from Seljak & Warren (2004), obtained from simulations of a ΛCDM universe, we infer an average host halo mass $\log_{10} M/{\rm M}_\odot \approx 12.1^{+0.5}_{-\infty}$ (or a 2σ upper limit $\log_{10} M/{\rm M}_\odot \lesssim 12.8$) for the full H-ATLAS sample. We find very similar values for the faint H-ATLAS subsample, $\log_{10} M/{\rm M}_\odot \approx 12.0^{+0.71}_{-\infty}$ (or a 2σ upper limit $\log_{10} M/{\rm M}_\odot \lesssim 13.0$). For the bright H-ATLAS sample, the average halo mass is $\log_{10} M/{\rm M}_\odot \approx 13.6^{+0.3}_{-0.4}$. The more luminous H-ATLAS galaxies thus appear to be hosted in significantly more massive haloes than the faint ones. Note that, given the large errors in the estimates of halo masses, it is reasonable that the 2σ upper limits on the host masses of the faint and bright subsamples are both higher than that of the full sample.

4 CONCLUSIONS

We have used a subset of the H-ATLAS galaxies in the SDP field, which have spectroscopic redshifts from the optical GAMA redshift survey, to calculate the projected cross-correlation functions of far-IR and optically selected galaxies. We find that these H-ATLAS galaxies (which have a median redshift $z \approx 0.2$, median 250 μm luminosity $L_{250} \approx 2.5 \times 10^{24}$ W Hz^{-1} and median total IR luminosity $L_{\rm IR} \sim 5.0 \times 10^{10}\,{\rm L}_\odot$) are significantly less strongly clustered than the optically selected GAMA galaxies (which have a median absolute magnitude, $M_r = -21.5$ mag) at the same redshifts. This effect is also seen (though with lower significance) in the autocorrelations of the H-ATLAS and GAMA galaxies.

From the cross-correlation analysis, combined with the previously measured clustering of optical galaxies in the SDSS, we find that H-ATLAS galaxies are less clustered than the dark matter, with an average bias $b = 0.71 \pm 0.09$. This implies a typical host halo mass of $\sim 1.25 \times 10^{12}\,{\rm M}_\odot$ for the H-ATLAS galaxies in our sample (which are mostly at low redshift), comparable to the halo of the Milky Way. These preliminary results for the host halo masses of the H-ATLAS galaxies are consistent with the theoretical predictions of Lacey et al. (2010) who find a typical halo mass of $1.6 \times 10^{12}\,{\rm M}_\odot$. [Note that Lacey et al. (2010) used the halo bias formula of Sheth, Mo & Tormen (2001), which predicts a somewhat larger bias than the Seljak & Warren (2004) formula used here at low masses.]

We also split our H-ATLAS sample into subsamples of high and low far-IR luminosity, and investigate their clustering properties. Both the cross- and auto-correlation functions suggest a dependence of clustering on far-IR luminosity over the range $L_{\rm IR} = 2.5 \times 10^{10}$–$7.9 \times 10^{10}\,{\rm L}_\odot$, with the bright galaxies being more strongly clustered than the faint ones at 2σ significance, implying that the more luminous galaxies are hosted by more massive dark haloes. The average halo mass for the bright sample is around $4 \times 10^{13}\,{\rm M}_\odot$ and the 2σ upper limit for the haloes hosting the faint sample is $10^{13}\,{\rm M}_\odot$. The dependence of clustering on far-IR luminosity that we find here appears significantly stronger than the model predictions of Lacey et al. (2010) who find $M_{\rm halo} \sim 1.3 \times 10^{12}$ and $2.0 \times 10^{12}\,{\rm M}_{\odot}$ for galaxies of comparable luminosities to our faint and bright subsamples. It will be interesting to test whether this discrepancy persists in the full H-ATLAS survey. As luminosity and redshift are correlated in a flux-limited sample, our high L_{250} luminosity subset has a higher median redshift than its fainter counterpart. Hence, in principle, strong evolution of clustering with redshift could be contributing to our inferred dependence of clustering on luminosity. We will be able to directly address this ambiguity with the much larger full H-ATLAS sample by splitting the sample into redshift bins. When completed, this survey will enable comprehensive investigations of the clustering and environments of star-forming galaxies.

ACKNOWLEDGMENTS

CSF acknowledges a Royal Society Wolfson Research Merit award. SC acknowledges the support of the Leverhulme Research Fellowship. This work was supported in part by a rolling grant from the Science and Technology Facilities Council to the ICC. The H-ATLAS survey[3] is being carried with ESA's *Herschel Space Observatory*, which is equipped with instruments provided by European-led Principal Investigator consortia, with important participation from the NASA, USA. Authors acknowledge support provided by the NASA through JPL. The GAMA[4] is a joint European–Australian spectroscopic campaign using the Anglo-Australian Telescope. The GAMA input catalogue is based on data from the SDSS and the UKIRT Infrared Deep Sky Survey. Complementary imaging of the GAMA regions is being obtained by a number of independent surveys, including *GALEX* MIS, VST KIDS, VISTA VIKING, *WISE*, H-ATLAS, GMRT and ASKAP, providing UV to radio coverage. PN acknowledges the support of a Royal Society University Research Fellowship. We thank Douglas Scott for a critical reading of our manuscript.

[3] http://www.h-atlas.org/
[4] http://www.gama-survey.org/

REFERENCES

Amblard A. et al., 2010, A&A, 518, L9
Baldry I. K. et al., 2010, MNRAS, 404, 86
Blanton M. R. et al., 2003, ApJ, 592, 819
Brinchmann J., Charlot S., White S. D. M., Tremonti C., Kauffmann G., Heckman T., Brinkmann J., 2004, MNRAS, 351, 1151
Ciliegi P., Zamorani G., Hasinger G., Lehmann I., Szokoly G., Wilson G., 2003, A&A, 398, 901
Cooray A. et al., 2010, A&A, 518, L22
Davis M., Peebles P. J. E., 1983, ApJ, 267, 465
Devlin M. J. et al., 2009, Nat, 458, 737
Driver S. P. et al., 2009, Astron. Geophys., 50, 050000
Driver S. P. et al., 2010, preprint (arXiv:1009.0614)
Dye S. et al., 2010, A&A, 518, L10
Eales S. et al., 2010, PASP, 122, 499
Griffin M. J. et al., 2010, A&A, 518, L3
Hamilton A. J. S., 1993, ApJ, 417, 19
Heinis S. et al., 2009, ApJ, 698, 1838
Hill D. T. et al., 2010, MNRAS, in press (doi:10.1111/j.1365-2966.2010.17950.x)
Lacey C. G., Baugh C. M., Frenk C. S., Benson A. J., Orsi A., Silva L., Granato G. L., Bressan A., 2010, MNRAS, 405, 2
Lewis I. et al., 2002, MNRAS, 334, 673
Li C., White S. D. M., 2009, MNRAS, 398, 2177
Maddox S. J. et al., 2010, A&A, 518, L11
Mo H. J., White S. D. M., 2002, MNRAS, 336, 112
Norberg P., Baugh C. M., Gaztañaga E., Croton D. J., 2009, MNRAS, 396, 19
Norberg P., Gaztañaga E., Baugh C. M., Croton D. J., 2011, MNRAS, submitted
Pascale E. et al., 2010, preprint (arXiv:1010.5782)
Pilbratt G. L. et al., 2010, A&A, 518, L1
Rigby E. E. et al., 2010, preprint (arXiv:1010.5787)
Robotham A. et al., 2010, PASA, 27, 76
Salim S. et al., 2007, ApJS, 173, 267
Seljak U., Warren M. S., 2004, MNRAS, 355, 129
Sheth R. K., Mo H. J., Tormen G., 2001, MNRAS, 323, 1
Smith D. J. B. et al., 2010, preprint (arXiv:1007.5260)
Sutherland W., Saunders W., 1992, MNRAS, 259, 413
Viero M. P. et al., 2009, ApJ, 707, 1766
Zehavi I. et al., 2010, preprint (arXiv:1005.2413)

This paper has been typeset from a TEX/LATEX file prepared by the author.